33rd Annual International Conference of the IEEE EMBS
Boston, Massachusetts USA, August 30 - September 3, 2011

Patient-Specific Modeling of Stress/Strain for Surgical Planning and Guidance

C. Sprouse[1], D. DeMenthon[1], J. Gammie[2], and P. Burlina[1,3]

Abstract— **We describe a method for performing modeling and simulation to predict the strain and stress experienced by tissues resulting from reconstructive cardiothoracic surgery. Stress computation is an important predictor of the quality and longevity of a repair and can therefore be used as guidance by a surgeon when deciding between various repair options. This paper uses the mitral valve repair as a use case because of its relevance and prevalence among reconstructive cardiac interventions. The modeling method presented here is informed by the patient specific anatomical structure recovered from real time 3D echocardiography. The method exploits hyperelastic models to infer realistic strain-stresses. We show through experiments using actual clinical data that results are in line with physiological expectations.**

I. Introduction

Modeling and simulation has many applications ranging from diagnostics to computer-aided surgical planning and guidance. Our work is motivated by the challenges encountered in cardiac surgical interventions, which are mostly reconstructive in nature. Among all cardiovascular diseases, the test case considered here is mitral valve reconstruction (valvuloplasty) because of its clinical relevance and surgical prevalence.

Most interventions for cardiovascular diseases (CVD) would benefit from pre-operative planning, by allowing the surgeon to evaluate the risks and benefits associated with a specific surgical option. Such systems would allow the surgeon to evaluate the quality of the reconstructive procedure by inspecting the resulting predicted postoperative anatomy and physiology (as was done in [1], [2]). Another benefit of the preoperative predictive planning is in examining the range of strains and stresses experienced by the reconstructed organ to assess the quality of the repair. Such quantities are also indicative and predictive of the longevity of the reconstruction. This is an important factor when considering the postoperative mortality and morbidity associated with procedures such as valvuloplasty [3].

While there is a large body of work in cardiac mechanical modeling (starting with [4] and including recent examples such as [1], [2], [5], [6], [7], [8]), until recently most of it has not exploited patient specific information for surgical planning and guidance. The recent availability of real time echographic 3D data has made possible the goal of cardiac modeling and simulation using patient-specific anatomy, as well as the possibility of benchmarking the predictive modeling against ground truth datasets [1], [2], [9]. The main contribution of this paper is the joint use of hyperelastic models and patient specific anatomy to predict the closure state and the stresses associated with a specific valve repair. Our models use a static loading method [10], [11], and incorporate physiological loads and realistic hyperelastic properties of valve soft tissues [6], [12]. Additionally, our modeling is informed by the patient specific anatomy of the valve and left heart apparatus recovered from real time 3D echocardiography (RT3DE). The benefits of this modality include its small size, safety, low cost, and high acquisition rate, a key factor when imaging rapid valvular motion. In our test study (valvuloplasty), a pre-operative simulation exploiting 3D anatomy recovered from 3D TEE would help decide which reconstructive option is most likely to improve the valve performance, and would provide information that is of critical aid to cardiovascular surgeons and cardiologists. The envisioned planning process starts with an open 3D valve structure at diastole, derived by segmenting RT3DE imagery and edited by a surgeon to remove artifacts and reflect the planned surgical modifications. From the open valve, our system predicts, via physics-based modeling and simulation, the closed valve configuration at systole to characterize the MV leaflets' ability to competently coapt, and the associated strains and stresses at systole for this closed configuration, when the system is under systolic blood load.

II. Quasi-Static MV Physics-based Modeling

Unlike our prior work in [1], which was concerned with computation of the valve dynamics and left heart hemodynamics, our goal here is to design a physics-based MV model to infer stresses and strains at the closed position of the valve (during systole) based on the open position valve configuration (during diastole). We use a shape-finding finite element approach previously applied to tensile structures [10], [11]. We have chosen this approach because the valve leaflets are thin structures made up of connective tissue with elastic properties (tensile, compressive and bending) similar to certain types of fabric; additionally, the valve behaves like a tensile structure since its leaflets are tethered by chords (chordae tendineae) attached to papillary muscles, preventing these from prolapsing into the atrium under sustained and significant systolic blood pressure. Unlike our preliminary work reported in [2], which used linear elastic constitutive models, this work uses a hyperelastic tissue model to infer resultant stresses [6], [12].

Manuscript received March 26, 2011, revised manuscript received June 20, 2011

[1]The Johns Hopkins University Applied Physics Laboratory, Laurel, MD 20723, [2]University of Maryland Heart Center, Baltimore, MD 21201, and [3]The Johns Hopkins University Computer Science Department, Baltimore, MD 21218

We start our process by segmenting the left heart endocardial and valvular structure from RT3DE using dynamic contour and graph optimization techniques, reported in [13]. A mesh is then fitted to the segmented leaflets and lower atrium. At each node of the mesh we prescribe either displacements or forces. Modeled forces include those due to fluid pressure, hyperelastic stress, collision with other portions of the mesh, and tethering of the valve to the chordae tendineae. The initial configuration of the open mesh is used to specify the reference energy point for external and internal forces. The steady state configuration of the valve system under load at a closed position, where all forces are at equilibrium, is then found by minimizing the system's total energy. For any given displacement of the nodes from the initial open configuration (see Fig. 1), and for each node i, the total energy ϕ of the displaced system is given by $\phi = \sum_i \phi_i$ with the forces $\mathbf{F}_i = -\nabla\phi_i$. Specifically, the energy is expressed as the sum of components in $\phi_i = \phi_i^X + \phi_i^E + \phi_i^T + \phi_i^C$ including: ϕ_i^X, the external energy; ϕ_i^E, the leaflets' elastic energy; ϕ_i^T, the leaflet-to-chordae tethering energy; and ϕ_i^C the leaflets' collision energy. The various energy terms are reported in [2]. The following section concentrates on the novel usage of a hyperelastic energy law for the leaflets' internal energy.

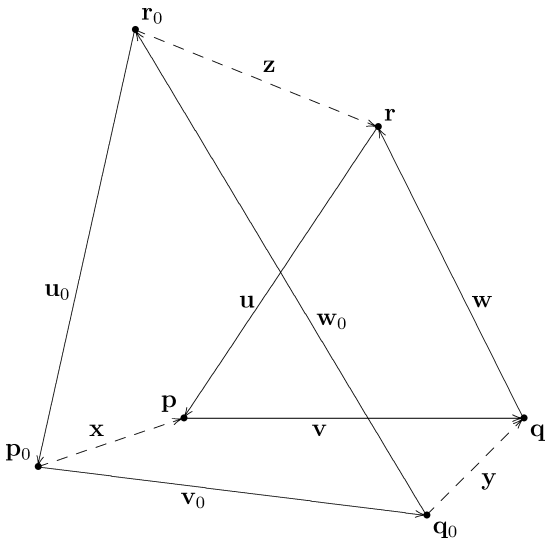

Fig. 1. Reference (subscripted) and deformed (unsubscripted) configuration. The vectors $\mathbf{x}$, $\mathbf{y}$, and $\mathbf{z}$ represent the nodal displacements.

The macroscopic mechanical behavior of the valve leaflets are mostly driven, at the microscopic level, by the elastic behavior of its constitutive elastin and collagen fibres [8]: Due to the presence of collagen fibres, the leaflets have some ability to stretch that arises when pressure is exerted on the collagen coils. Because of this, we have chosen to model the leaflet elasticity using a hyperelastic strain-energy law. In this paper, we use a law proposed by Holzapfel [6] which is closely related to a constitutive law originally formulated by May-Newman [12] and based on empirical evidence. This hyperelastic energy law is expressed as:

$$\Psi(I_1, I_4) = c_0 \left[e^{c_1(I_1-3)^2 + c_2(I_4-1)^2} - 1 \right], \qquad (1)$$

and it is a function of the first and fourth invariants of the strain tensor $\mathbf{C}$ (i.e., $I_1 = \mathrm{tr}\,(\mathbf{C})$ and $I_4 = \widehat{\mathbf{a}}_0^{\mathrm{T}}\mathbf{C}\widehat{\mathbf{a}}_0$ is the square of the stretch factor along the fibre direction). The fibre direction was taken to be circumferential to the annulus [14]. The numerical values we have used for the parameters in this hyperelastic strain energy function were taken from [6], and were derived to match the empirical leaflet elasticity data in [12]: $c_0 = 0.0520$ kPa, $c_1 = 4.63$, and $c_2 = 22.6$ for the anterior leaflet, and $c_0 = 0.171$ kPa, $c_1 = 5.28$, and $c_2 = 6.46$ for the posterior leaflet. These values were obtained by considering leaflet samples from taken from eight porcine MV specimens among which there was considerable variation. This, along with significant loss of plasticity and elasticity in pathological tissue, suggests the need to investigate in the future the recovery of patient specific values for these coefficients. Fig. 2 shows the Cauchy stress as a function of the stretch for the numerical values of the coefficients defined above and for various cases including strip-biaxial and biaxial stretching.

The derivation of the force from the hyperelastic energy is needed by our quasi-Newton minimization approach. This derivation is an important component of our mechanical modeling framework. Since it is not available in the literature in the form needed by our modeling framework, we dedicate the next paragraphs to its presentation. To simplify notation, we will omit the node subscript index i, with the understanding that each quantity (stress, strain tensors, etc.) is computed w.r.t. each node of the model.

The deformation gradient tensor, $\mathbf{F}$, gives the transformation between the reference and deformed configurations shown in Fig. 1. This transformation consists of a rigid rotation, $\mathbf{R}$, and a symmetric stretch tensor, $\mathbf{U}$, with $\mathbf{F} = \mathbf{RU}$. This decomposition may also be performed in the opposite order such that $\mathbf{F} = \mathbf{VR}$. Since the rotation $\mathbf{R}$ is not physically significant, the right and left Cauchy-Green deformation tensors, $\mathbf{C} \equiv \mathbf{F}^{\mathrm{T}}\mathbf{F} = \mathbf{U}^2$ and $\mathbf{B} \equiv \mathbf{F}\mathbf{F}^{\mathrm{T}} = \mathbf{V}^2$ respectively, provide a more useful measure of deformation. For a triangular patch of a thin-shell membrane, $\mathbf{F}$ transforms the triangle in the reference configuration (defined by the vertices $\mathbf{x}_0$, $\mathbf{y}_0$, $\mathbf{z}_0$; opposing edges $\mathbf{u}_0$, $\mathbf{v}_0$, $\mathbf{w}_0$; and normal $\mathbf{n}_0$) into the deformed configuration (same vectors without subscript) as

$$\mathbf{u} = \mathbf{F}\mathbf{u}_0 \qquad \mathbf{w} = \mathbf{F}\mathbf{w}_0 \qquad (2)$$

$$\mathbf{v} = \mathbf{F}\mathbf{v}_0 \qquad \mathbf{n} = \alpha\widehat{\mathbf{n}} = \mathbf{F}\widehat{\mathbf{n}}_0, \qquad (3)$$

where $\alpha \equiv |\mathbf{n}|$ is the stretch factor in the direction normal to the facet. We will also define two orthogonal reference directions in the plane of the facet $\widehat{\mathbf{a}}_0$ and $\widehat{\mathbf{b}}_0$ with $\widehat{\mathbf{n}}_0 = \widehat{\mathbf{a}}_0 \times \widehat{\mathbf{b}}_0$. These vectors are transformed by $\mathbf{F}$ into $\mathbf{a} = \mathbf{F}\widehat{\mathbf{a}}_0$ and $\mathbf{b} = \mathbf{F}\widehat{\mathbf{b}}_0$ with corresponding stretch factors $\lambda = |\mathbf{a}|$ and $\mu = |\mathbf{b}|$. For an incompressible material, we have the condition

$$\det \mathbf{F} = 1, \qquad (4)$$

which fixes the value of α and thus completes the specifica-

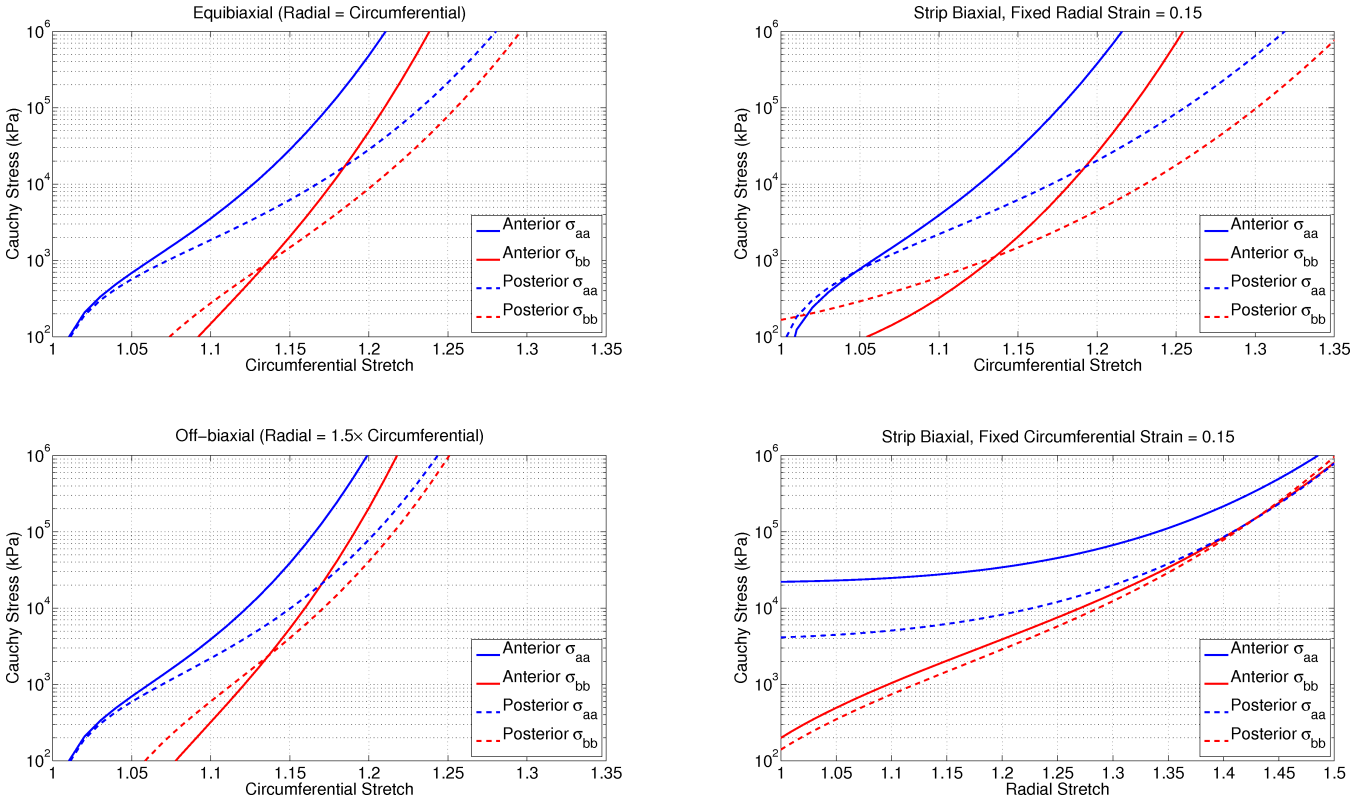

Fig. 2. A plot of the Cauchy stress vs. stretch of the valve for our hyperelastic model.

tion of $\mathbf{F}$. Without loss of generality, define the matrices

$$\mathbf{G}_0 \equiv \mathbf{u}_0\widehat{\mathbf{e}}_1^{\mathrm{T}} + \mathbf{v}_0\widehat{\mathbf{e}}_2^{\mathrm{T}} + \widehat{\mathbf{n}}_0\widehat{\mathbf{e}}_3^{\mathrm{T}}, \text{ and} \tag{5}$$

$$\mathbf{G} \equiv \mathbf{u}\widehat{\mathbf{e}}_1^{\mathrm{T}} + \mathbf{v}\widehat{\mathbf{e}}_2^{\mathrm{T}} + \mathbf{n}\widehat{\mathbf{e}}_3^{\mathrm{T}}, \tag{6}$$

such that $\mathbf{F} = \mathbf{G}\mathbf{G}_0^{-1}$. The condition (4) then gives $\alpha = A_0/A$, where $A_0 \equiv |\mathbf{u}_0 \times \mathbf{v}_0|$ and $A \equiv |\mathbf{u} \times \mathbf{v}|$. This yields an explicit representation for $\mathbf{n}$,

$$\mathbf{n} = \alpha\widehat{\mathbf{n}} = \frac{|\mathbf{u}_0 \times \mathbf{v}_0|}{|\mathbf{u} \times \mathbf{v}|}\frac{\mathbf{u} \times \mathbf{v}}{|\mathbf{u} \times \mathbf{v}|} = \frac{A_0}{A^2}\mathbf{u} \times \mathbf{v}. \tag{7}$$

Let $\widehat{\mathbf{a}}_0$ be the fibre direction in the reference configuration (this generally corresponds to a direction circumferential to the annulus), then the stretch factor along $\mathbf{a}$ is given by

$$\lambda^2 \equiv |\mathbf{a}|^2 = \widehat{\mathbf{a}}_0^{\mathrm{T}}\mathbf{F}^{\mathrm{T}}\mathbf{F}\widehat{\mathbf{a}}_0 = \widehat{\mathbf{a}}_0^{\mathrm{T}}\mathbf{C}\widehat{\mathbf{a}}_0 \equiv I_4. \tag{8}$$

The second Piola-Kirchhoff stress tensor $\mathbf{S}$ is

$$\mathbf{S} = 2\psi_1\mathbf{1} + 2\psi_4\widehat{\mathbf{a}}_0\widehat{\mathbf{a}}_0^{\mathrm{T}} - p\mathbf{C}^{-1} \equiv \mathbf{S}' - p\mathbf{C}^{-1}, \tag{9}$$

where $I_1 = \operatorname{tr}\mathbf{C}$ and $\psi_i \equiv \partial\Psi/\partial I_i$, with

$$\psi_1 = 2c_0c_1(I_1 - 3)e^{c_1(I_1-3)^2 + c_2(I_4-1)^2}, \text{ and} \tag{10}$$

$$\psi_4 = 2c_0c_2(I_4 - 1)e^{c_1(I_1-3)^2 + c_2(I_4-1)^2}, \tag{11}$$

and from the condition that the normal stress is zero ($\widehat{\mathbf{n}}_0^{\mathrm{T}}\mathbf{S}\widehat{\mathbf{n}}_0 = 0$) we have

$$p = \frac{\widehat{\mathbf{n}}_0^{\mathrm{T}}\mathbf{S}'\widehat{\mathbf{n}}_0}{\widehat{\mathbf{n}}_0^{\mathrm{T}}\mathbf{C}^{-1}\widehat{\mathbf{n}}_0} = \frac{2\psi_1}{\widehat{\mathbf{n}}_0^{\mathrm{T}}\mathbf{C}^{-1}\widehat{\mathbf{n}}_0} = \frac{2\psi_1}{|\mathbf{F}^{-\mathrm{T}}\widehat{\mathbf{n}}_0|^2} = 2\psi_1\alpha^2, \tag{12}$$

which gives

$$\mathbf{S} = 2\psi_1(\mathbf{1} - \alpha^2\mathbf{C}^{-1}) + 2\psi_4\widehat{\mathbf{a}}_0\widehat{\mathbf{a}}_0^{\mathrm{T}}. \tag{13}$$

The Cauchy stress is a commonly referenced quantity and is given by $\boldsymbol{\sigma} = \mathbf{F}\mathbf{S}\mathbf{F}^{\mathrm{T}}$. We are interested in the components of $\boldsymbol{\sigma}$ in the directions parallel and perpendicular to $\mathbf{a}$,

$$\sigma_{\mathrm{aa}} = 2\psi_1\left[\frac{|\mathbf{C}\widehat{\mathbf{a}}_0|^2}{\lambda^2} - \alpha^2\right] + 2\psi_4\lambda^2, \tag{14}$$

$$\sigma_{\mathrm{bb}} = 2\psi_1\left[\frac{|\mathbf{C}\widehat{\mathbf{b}}_0|^2}{\mu^2} - \alpha^2\right] + 2\psi_4\frac{(\widehat{\mathbf{a}}_0^{\mathrm{T}}\mathbf{C}\widehat{\mathbf{b}}_0)^2}{\mu^2}, \tag{15}$$

$$\sigma_{\mathrm{ab}} = 2\psi_1\left[\frac{\widehat{\mathbf{a}}_0^{\mathrm{T}}\mathbf{C}^2\widehat{\mathbf{b}}_0}{\lambda\mu} - \alpha^2\frac{\widehat{\mathbf{a}}_0^{\mathrm{T}}\mathbf{C}\widehat{\mathbf{b}}_0}{\lambda\mu}\right] + 2\psi_4\lambda\frac{\widehat{\mathbf{a}}_0^{\mathrm{T}}\mathbf{C}\widehat{\mathbf{b}}_0}{\mu}. \tag{16}$$

From the strain energy, Ψ, the force on each vertex is given

by

$$\begin{aligned}\nabla\Psi &= 2\psi_1\left[\alpha^2\frac{\mathbf{u}\cdot\mathbf{v}}{A^2}-\frac{\mathbf{u}_0\cdot\mathbf{v}_0}{A_0^2}\right](a\mathbf{v}+b\mathbf{u})\\ &+2\psi_1\left[\frac{|\mathbf{v}_0|^2}{A_0^2}-\alpha^2\frac{|\mathbf{v}|^2}{A^2}\right]a\mathbf{u}\\ &+2\psi_1\left[\frac{|\mathbf{u}_0|^2}{A_0^2}-\alpha^2\frac{|\mathbf{u}|^2}{A^2}\right]b\mathbf{v}\\ &+2\psi_4\frac{(\widehat{\mathbf{a}}_0\cdot\mathbf{u}_0)(\widehat{\mathbf{a}}_0\cdot\mathbf{v}_0)-(\mathbf{u}_0\cdot\mathbf{v}_0)}{A_0^2}(a\mathbf{v}+b\mathbf{u})\\ &+2\psi_4\frac{|\mathbf{v}_0|^2-(\widehat{\mathbf{a}}_0\cdot\mathbf{v}_0)^2}{A_0^2}a\mathbf{u}\\ &+2\psi_4\frac{|\mathbf{u}_0|^2-(\widehat{\mathbf{a}}_0\cdot\mathbf{u}_0)^2}{A_0^2}b\mathbf{v}, \end{aligned}\tag{17}$$

where $(a,b)=(1,-1),(0,1),(-1,0)$ for the displacements $\mathbf{x}$, $\mathbf{y}$, $\mathbf{z}$ respectively. This provides an analytical expression for the force which can be used in a gradient descent, Newton-Raphson, or quasi-Newton minimization process.

The variation of total potential energy is a function of $3N$ displacement coordinates where N is the number of free nodes. To find the closed position of the leaflets given the distributed forces and imposed displacements, we find the configuration which minimizes the total energy by using the BFGS (Broyden Fletcher Goldfarb Shanno) quasi-Newton optimization process.

III. Experiments

Our data consist of an intraoperative RT3DE transesophageal full volume sequence of the left heart. The RT3DE acquisition was performed using an iE33 Philips console with a Philips X2-T Live probe (Philips Medical Systems, Bothell, WA). The RT3DE cube sizes were 208×208×224. The RT3DE probe was operated at frequencies ranging from 3 to 5 MHz and frame rate of 50 Hz. The pixels' spatial resolutions were respectively 0.666×0.657×0.580 mm or approximately 1.10 mm diagonal voxel resolution. A 7 breath-hold cycle acquisition protocol was employed leading to a frame rate of close to 50 Hz. We performed automated valve and endocardial wall segmentation as described in [13]. This was followed by expert review and correction to edit out artifacts and to complete any missing anatomical structures due to reverberation, self obscuration of the valve, and limitations of the RT3DE field of view. The positioning of the valve annulus, tether connections, and papillary muscles were specified from visual inspection of the RT3DE. The numerical parameter values were specified as indicated in the previous section.

Benchmarking was performed using two RT3DE cases and was carried out by computing absolute errors between (a) the closed valve configuration predicted at systole from the segmented open valve captured at diastole, and (b) the closed valve segmented during systole. Manual adjustment of the overall vertical translation of the predicted valve was made to compensate for the mostly single axis translational motion of the annulus, which is not considered in our model. Similarly, compensation for the dilation of the annulus between diastole and systole was performed based on empirical dilation measurements reported in [15]. We found on average a mean absolute error of 2.9 mm with std. dev. 2.6 mm for case 1 and 3.3 mm and 3.0 mm respectively for case 2.

Fig. 3 shows the convergence of the minimization process to the computed closed configuration. Color coded areas correspond the anterior (red) and posterior (blue) leaflets and include sections of the attached primary chordae tendineae. The green region includes the annulus as well as the lower part of the atrium which remain static in the minimization process. The RT3DE-based closed state simulations resulted in physiological strains and plausible stresses: stretching as measured by fractional area change averaged 39%. Mean average Cauchy stresses for the posterior leaflet were 56 kPa circumferential and 146 kPa radial. The values were respectively 68 kPa and 113 kPa for the anterior leaflet. 95th percentile stresses for the posterior leaflet were 209 kPa circumferential and 534 kPa radial. The values were 284 kPa and 430 kPa respectively for the anterior leaflet. Those values are consistent with findings in other modeling and empirical studies [7], [8], [12], [16].

IV. Conclusions

We describe a novel RT3DE-guided physics-based modeling and simulation procedure to predict the stresses and strains for a closed state MV from an open MV configuration exploiting a static load analysis and optimization and using realistic physiological load and hyperelastic anisotropic forces. Testing with clinical data shows the ability to predict stress/strain values that are consistent with prior findings. This load analysis will allow surgeons to evaluate the quality and predict the longevity of candidate procedures.

Acknowledgments

We wish to thank Profs. D. Yuh (JHMI/Cardiothoracic Surgery), E. McVeigh (JHU BME), T. Abraham, and A. Pinheiro (JHMI/Cardiology) for help in data acquisition and useful discussions. This project was supported in part by JHU APL Science and Technology Research and Development funds and by NIH NHLBI R21HL098765. The content is solely the responsibility of the authors and does not necessarily represent the official views of the National Heart, Lung, And Blood Institute or the National Institutes of Health.

References

[1] C. Sprouse, D. Yuh, T. Abraham, and P. Burlina, "Computational hemodynamic modeling based on transesophageal echocardiographic imaging," *Proc. Int. Conf. Engineering in Medicine and Biology Society*, vol. 2009, pp. 3649–3652, 2009.

[2] P. Burlina, C. Sprouse, D. DeMenthon, A. Jorstad, R. Juang, F. Contijoch, T. Abraham, D. Yuh, and E. McVeigh, "Patient-specific modeling and analysis of the mitral valve using 3D-TEE," *Information Processing in Computer-Assisted Interventions*, pp. 135–146, 2010.

[3] J. Gammie, S. O'Brien, B. Griffith, T. Ferguson, and E. Peterson, "Influence of hospital procedural volume on care process and mortality for patients undergoing elective surgery for mitral regurgitation," *Circulation*, vol. 115, no. 7, p. 881, 2007.

[4] C. Peskin, "Numerical analysis of blood flow in the heart," *Journal of Computational Physics*, vol. 25, no. 3, pp. 220–252, 1977.

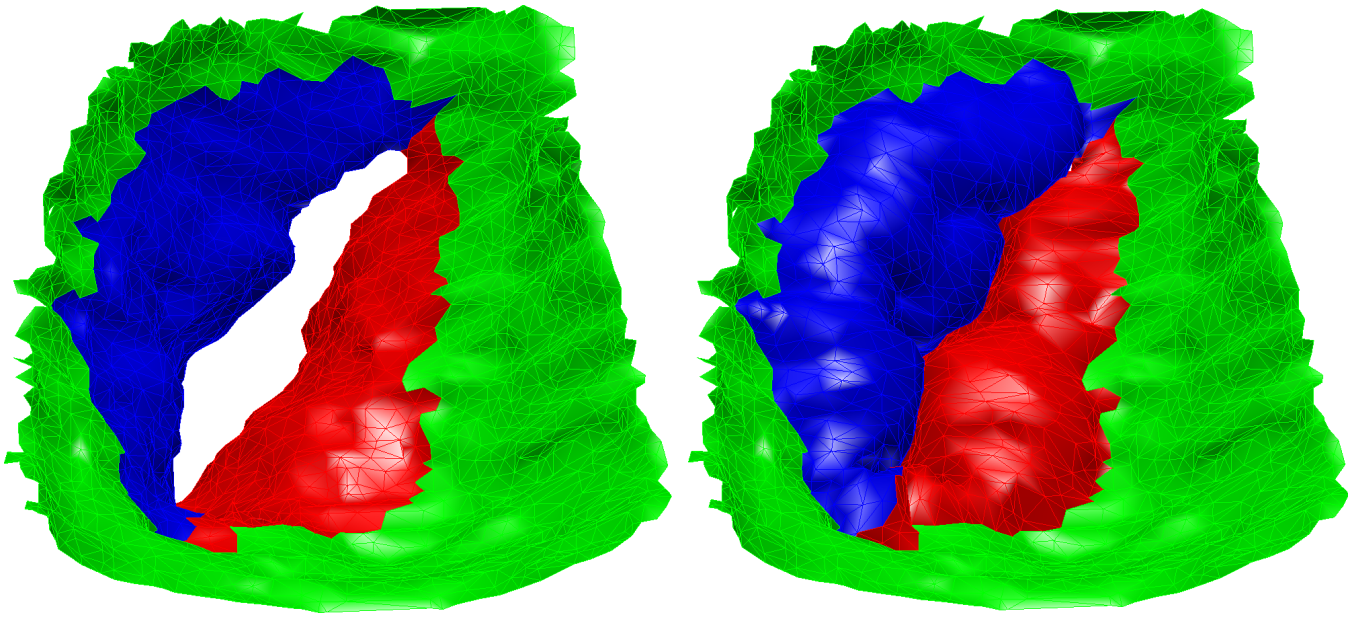

Fig. 3. Measured open-valve configuration obtained by segmentation of a single instant RT3DE observation (left). Computed closed-valve configuration (right). Anterior MV leaflet indicated in red, posterior leaflet in blue, and annulus plus lower atrium in green.

[5] M. Sacks, Y. Enomoto, J. Graybill, W. Merryman, A. Zeeshan, A. Yoganathan, R. Levy, R. Gorman, and J. Gorman, "In-Vivo Dynamic Deformation of the Mitral Valve Anterior Leaflet," *The Annals of Thoracic Surgery*, vol. 82, pp. 1369–1377, 2006.

[6] V. Prot, B. Skallerud, and G. Holzapfel, "Transversely isotropic membrane shells with application to mitral valve mechanics. Constitutive modelling and finite element implementation," *Int. Journal for Numerical Methods in Engineering*, vol. 71, no. 8, pp. 987–1008, 2007.

[7] D. Einstein, F. Del Pin, X. Jiao, A. Kuprat, J. Carson, K. Kunzelman, R. Cochran, J. Guccione, and M. Ratcliffe, "Fluid-structure interactions of the mitral valve and left heart: Comprehensive strategies, past, present and future," *Int. Journal for Numerical Methods in Biomedical Engineering*, vol. 26, no. 3-4, pp. 348–380, 2010.

[8] E. Votta, E. Caiani, F. Veronesi, M. Soncini, F. Montevecchi, and A. Redaelli, "Mitral valve finite-element modelling from ultrasound data: a pilot study for a new approach to understand mitral function and clinical scenarios," *Philosophical Transactions of the Royal Society A: Mathematical, Physical and Engineering Sciences*, vol. 366, no. 1879, p. 3411, 2008.

[9] P. E. Hammer, D. P. Perrin, P. J. del Nido, and R. D. Howe, "Image-based mass-spring model of mitral valve closure for surgical planning," in *Proc. of SPIE*, San Diego, CA, USA, 2008, pp. 69 180Q–69 180Q–8.

[10] O. Le Maitre, S. Huberson, and S. De Cursi, "Unsteady model of sail and flow interaction," *Journal of Fluids and Structures*, vol. 13, pp. 37–60, 1999.

[11] F. Hauville, S. Mounoury, Y. Roux, and J. Astolfi, "Equilibre dynamique d'une structure idealement flexible dans un ecoulement: application a la deformation des voiles." *Journées AUM AFM 2004*, 2004.

[12] K. May-Newman and F. Yin, "A constitutive law for mitral valve tissue," *Journal of Biomechanical Engineering*, vol. 120, p. 38, 1998.

[13] P. Burlina, R. Mukherjee, C. Sprouse, and R. Juang, "Recovering endocardial walls from 3D TEE," in *Int. Conf. On Functional Imaging and Modeling of the Heart*, 2011.

[14] J. Grashow, A. Yoganathan, and M. Sacks, "Biaxial stress–stretch behavior of the mitral valve anterior leaflet at physiologic strain rates," *Annals of Biomedical Engineering*, vol. 34, no. 2, pp. 315–325, 2006.

[15] M. Herregods, A. Tau, A. Vandeplas, B. Bijnens, and F. WERF, "Values for mitral valve annulus dimensions in normals and patients with mitral regurgitation," *Echocardiography*, vol. 14, no. 6, pp. 529–533, 1997.

[16] E. Votta, F. Maisano, S. Bolling, O. Alfieri, F. Montevecchi, and A. Redaelli, "The geoform disease-specific annuloplasty system: a finite element study," *The Annals of thoracic surgery*, vol. 84, no. 1, pp. 92–101, 2007.